Article

Progress in Physical Geography
001–22

DOI: 10.1177/0309133313496835
ppg.sagepub.com
SAGE

Sea-level rise vulnerability mapping for adaptation decisions using LiDAR DEMs

Hannah M. Cooper
University of Hawai'i, USA

Charles H. Fletcher
University of Hawai'i, USA

Qi Chen
University of Hawai'i, USA

Matthew M. Barbee
University of Hawai'i, USA

Abstract
Global sea-level rise (SLR) is projected to accelerate over the next century, with research indicating that global mean sea level may rise 18–48 cm by 2050, and 50–140 cm by 2100. Decision-makers, faced with the problem of adapting to SLR, utilize elevation data to identify assets that are vulnerable to inundation. This paper reviews techniques and challenges stemming from the use of Light Detection And Ranging (LiDAR) digital elevation models (DEMs) in support of SLR decision-making. A significant shortcoming in the methodology is the lack of comprehensive standards for estimating LiDAR error, which causes inconsistent and sometimes misleading calculations of uncertainty. Workers typically aim to reduce uncertainty by analyzing the difference between LiDAR error and the target SLR chosen for decision-making. The practice of mapping vulnerability to SLR is based on the assumption that LiDAR errors follow a normal distribution with zero bias, which is intermittently violated. Approaches to correcting discrepancies between vertical reference systems for land and tidal datums may incorporate tidal benchmarks and a vertical datum transformation tool provided by the National Ocean Service (VDatum). Mapping a minimum statistically significant SLR increment of 32 cm is difficult to achieve based on current LiDAR and VDatum errors. LiDAR DEMs derived from 'ground' returns are essential, yet LiDAR providers may fail to remove returns over vegetated areas successfully. LiDAR DEMs integrated into a GIS can be used to identify areas that are vulnerable to direct marine inundation and groundwater inundation (reduced drainage coupled with higher water tables). Spatial analysis can identify potentially vulnerable ecosystems as well as developed assets. A standardized mapping uncertainty needs to be developed given that SLR vulnerability mapping requires absolute precision for use as a decision-making tool.

Keywords
adaptation, DEM, error, LiDAR, sea-level rise, uncertainty, vulnerability mapping

Corresponding author:
Hannah M. Cooper, Department of Geology and Geophysics, School of Ocean and Earth Science and Technology, University of Hawai'i, 1680 East West Road, Honolulu, HI 96822, USA.
Email: hannahco@hawaii.edu

I Introduction

The rate of global sea-level rise (SLR) has accelerated from approximately 1.7 ± 0.3 mm/yr during the 20th century (Church and White, 2006) to about 3.2 ± 0.4 mm/yr at present (Church and White, 2011). It is estimated that roughly 10% of the world's population live within low-lying coastal areas below 10 m elevation (McGranahan et al., 2007). The threat posed by accelerated SLR to 'vulnerable' coastal systems (i.e. human and natural) compels scientists to achieve consensus on methodologies for mapping environmental change and assessing 'adaptation' options (e.g. NOAA, 2010a; Nicholls, 2011; Rahmstorf, 2012). Vulnerability is defined by the Intergovernmental Panel on Climate Change (IPCC, 2007: 883) as 'the degree to which a system is susceptible to, or unable to cope with, adverse effects of climate change'. Vulnerability to SLR may be viewed as a function of a coastal system's potential exposure (e.g. frequency of hazards), its sensitivity (e.g. level of damages caused by flooding), and its adaptive capacity (e.g. management policies; Adger, 2006). Adaptation may be referred to as a reaction based on an assessment of future conditions (Adger et al., 2005) due to SLR (e.g. SLR vulnerability maps). However, we acknowledge that adaptation can also be based on past or current conditions (Adger et al., 2005) due to other effects of SLR, such as salt-water intrusion into coastal aquifers (already a problem in southeastern Florida; Florida Oceans and Florida Coastal Council, 2010). Here we define SLR vulnerability mapping as a method of assessing the spatial distribution of the potential effects of future SLR. We recognize that these potential effects may include direct flooding by ocean waters (marine inundation), indirect flooding due to reduced drainage coupled with higher water tables (groundwater inundation; Rotzoll and Fletcher, 2013), saltwater intrusion, wetland loss, erosion, etc. SLR vulnerability mapping provides a cartographic tool for illustrating assets at risk that are therefore targets for adaptation decisions.

Generating reliable maps of low-lying, low-slope coastal systems vulnerable to the potential effects of future SLR primarily depends on the resolution and accuracy of the elevation data used to identify sensitive areas (e.g. Coveney and Fotheringham, 2011; Coveney et al., 2010; Gesch, 2009). Globally, the application of digital elevation models (DEMs) for generating SLR vulnerability maps and assessments has become a standard practice (e.g. Dawson et al., 2005; Hinkel et al., 2010; Marfai and King, 2008; Titus and Richman, 2001). However, the use of DEMs with elevation values quantized in whole meters, coarse horizontal resolution (e.g. 30 m), and high vertical uncertainty (e.g. root mean square error or RMSE at the order of meters) limits this methodology to illustrating broad impacts and is not ideal for planning (Gesch, 2009; Gesch et al., 2009; Kettle, 2012; Zhang, 2011). Raber et al. (2007) note that the more coarse the horizontal resolution of a DEM, the larger the map errors. Strauss et al. (2012) made explicit that the application of 10 m horizontal resolution DEMs was beneficial for demonstrating the general impacts of SLR, but not for generating detailed vulnerability maps. Brown (2006) used the best available elevation data derived from Interferometric Synthetic Aperture Radar (IfSAR) at a horizontal resolution of 5 m and vertical resolution of 50 cm. Kettle (2012) notes that obtaining high-resolution data and implementing the appropriate methodologies for quantifying SLR impacts remains a challenge. Because there is high demand for SLR decision-support tools using high-resolution DEMs (Hinkel and Klein, 2009), coastal elevations are more recently being measured by high-resolution state-of-the-art Light Detection And Ranging (LiDAR). DEMs built of LiDAR data are increasingly being used by decision-makers in forming management guidelines and to identify high-resolution SLR hazard zones (Brock and Purkis, 2009).

LiDAR is allowing researchers to generate more precise SLR vulnerability maps to aid adaptation decisions (e.g. Cooper et al., 2012; Webster et al., 2004; Zhang et al., 2011). For example, DEMs generated from LiDAR allow interpretation of vulnerable fine-scale terrain surface features (e.g. individual properties and buildings; Zhang, 2011). LiDAR DEMs provide improvements to delineating potential SLR impacts because elevation values are quantized in centimeters, horizontal resolution is high (e.g. 1 m), and vertical error is appropriately scaled (i.e. RMSE at the order of centimeters; Gesch, 2009; Webster et al., 2006). However, LiDAR data providers sometimes conduct 'in-house' error assessments (Hodgson et al., 2005) quoting a typical RMSE of 15 cm (Hodgson and Bresnahan, 2004). In reality, it is extremely difficult to achieve a low RMSE of 15 cm for land-cover types other than flat open terrain (Aguilar et al., 2010), and modeling inundation on natural coastal systems often involves coastal marshes and vegetated areas (e.g. Cooper et al., 2012; Hladik and Albers, 2012; Schmid et al., 2011). Limitations to using LiDAR include distinguishing between ground and vegetation, in which bald-earth products produced by data providers may sometimes remove tall trees, but not low, dense vegetation (Rosso et al., 2006). Furthermore, issues such as a lack of a common error standard for LiDAR, and discrepancies between vertical datums are challenging topics to generating high-resolution SLR vulnerability maps from LiDAR.

The purpose of this paper is to review technical developments and challenges to conducting research using LiDAR DEMs for SLR vulnerability mapping. The following section introduces future SLR estimates with a focus on identifying physical climate models, semi-empirical models, and observations. Section III reviews the various standards for assessing LiDAR error in relation to mapping vertical uncertainty, and the occasional false assumption that errors follow a normal distribution with zero bias. Section IV demonstrates approaches to discrepancies between the vertical land datum to which LiDAR is referenced and local tidal datums, in addition to the development of the vertical datum transformation tool VDatum. Mapping minimum statistically significant SLR scenarios is also discussed in section V. Issues regarding LiDAR point processing into 'ground' returns critical for generating LiDAR DEMs used in SLR vulnerability mapping are discussed in section VI. Section VII presents techniques of inundation modeling, highlighting recent developments in mapping direct marine inundation and groundwater inundation. Section VIII reviews techniques for evaluating vulnerability by sector, and section IX provides an example of best practices. The final section concludes the discussion while providing a summary about areas of future focus.

II SLR estimates

Choosing the appropriate SLR scenarios for implementing adaptation decisions depends on research progress published by the scientific community such as the National Research Council (NRC, 2012), although political and economic systems are also contributing factors. The reliability of SLR estimates becomes increasingly important when used to produce maps that assist in developing public policy. Thus there exists an urgent need to improve SLR projections based on advances in our understanding of the true causes of rising sea levels (Church et al., 2011).

Two major physical processes drive global SLR due to environmental change: thermal expansion of ocean waters, and release of land-based ice into the ocean (Meehl et al., 2007). Understanding and quantifying the effects of these processes, and their geographic variability and uncertainties, are a primary focus of SLR research. In their Fourth Assessment Report, the IPCC used physical climate models to estimate that global mean sea level (MSL) may rise an average 18–59 cm by the period 2090–2099

(Meehl et al., 2007) or 19–63 cm by 2100 (Church et al., 2011). It is understood that IPCC (2007) may underestimate global SLR because important contributions from ice sheet dynamics are excluded (e.g. Rahmstorf et al., 2007). Modeling the response of ice sheets to a changing environment remains a major challenge in estimating future SLR (e.g. Church et al., 2011; Rahmstorf, 2010; Slangen et al., 2012). Using a combination of model results and observations, researchers identified three global mean SLR planning targets: 8–23 cm by 2030, 18–48 cm by 2050, and 50–140 cm by 2100 (relative to 2000 levels; NRC, 2012).

Rahmstorf (2007) found that sea level might be responding to a warming climate faster than IPCC models project. He developed a semi-empirical model that was later improved (Vermeer and Rahmstorf, 2009) and assessed (Rahmstorf et al., 2011) to estimate that global MSL could rise 0.75–1.9 m by the end of the 21st century. Church et al. (2011) raised a concern about the Vermeer and Rahmstorf (2009) semi-empirical model lacking groundwater depletion. Rahmstorf et al. (2011) tested the robustness of various semi-empirical models and found that the best-estimate model, which also accounted for groundwater depletion, was almost identical to Vermeer and Rahmstorf (2009). Jevrejeva et al. (2010) also developed a semi-empirical model and were able to estimate a smaller range of uncertainty in SLR (0.6–1.6 m by 2100). Church et al. (2011) reasoned that poor understanding of the processes that cause SLR has led to the semi-empirical approach, but this is only a temporary and inadequate response to the problem. Using ice dynamics coupled with other processes, Pfeffer et al. (2008) projected a most probable rise of 80 cm by the end of the century. Rignot et al. (2011) extrapolated observations of temporal variations in the Greenland and Antarctic ice sheet mass balance, summed with thermal expansion of shallow seawater as calculated in AR4, and concluded that global mean sea level may rise 32 cm by the year 2050, an estimate that is consistent with Vermeer and Rahmstorf (2009) as well as NRC (2012). It is understood that regional SLR will likely differ from global mean SLR. Slangen et al. (2012) modeled regional variability of relative SLR using a combination of spatial patterns of steric effects, land ice melt, and glacial isostatic adjustment obtained from various models.

Future SLR, although exhaustively modeled by many researchers using a range of approaches and assumptions, remains very uncertain. However, decision-makers cannot adequately plan for adaptation to the most harmful effects without a reasonably well-justified target. It can be argued that under a scenario of warming and melting that has been observed in the past decade, research is converging on an estimate of approximately 1 m of SLR by 2100, making this an appropriate long-term target for planning and adaptation decision-making (e.g. Fletcher, 2009; NRC, 2012; Nicholls, 2011; Rahmstorf, 2010). This value is roughly consistent with the estimate of Pfeffer et al. (2008), and planning for a 1 m rise by 2100 is also consistent with the projection of 1.8–5.5 m by AD2500 (Jevrejeva et al., 2012). For an earlier target by the year 2050, Rignot et al. (2011) calculate that global mean sea level will rise approximately 32 cm. This is in the range of NRC (2012) projections, and constitutes a useful short-term target for adaptation planning. These planning targets focus attention on the capabilities of LiDAR elevation data to accurately depict lands vulnerable to 32 cm and 1 m of SLR. A thorough investigation of this issue requires a comprehensive understanding of elevation accuracy or errors associated with LiDAR and its processing.

III LiDAR error

1 Common sources of LiDAR error

There are many known causes that contribute to LiDAR error such as data collection, terrain slope, land-cover type, LiDAR sensor, and filtering methods. The three-dimensionality of

a LiDAR elevation data set is denoted by the coordinates *x* and *y* for horizontal positions, and the letter *z* for vertical positions. Sources of LiDAR positional error (*xyz*) in data collection include the global positioning system (GPS) that records the aircraft's *xyz* position, the inertial measurement unit (IMU) for monitoring the aircraft's attitude (yaw, pitch, roll), and the ranging and direction of the laser beam (Hodgson and Bresnahan, 2004; Shen and Toth, 2009). A steep terrain slope will also cause LiDAR *xy* errors that influence LiDAR *z* errors (NDEP, 2004). However, Hodgson et al. (2005) observed little evidence that LiDAR error increased in low slopes typical of flood zones (0–8°). Instead, they found that LiDAR *z* error is highly influenced by land-cover type (e.g. low and high vegetation). Hladik and Alber (2012) demonstrate that despite recent technological advances in GPS and IMU, and the LiDAR sensor having better laser penetration through vegetation due to higher pulse rate frequencies (PRF; i.e. laser point density), state-of-the-art high PRF LiDAR is limited to detecting bare earth in coastal marsh areas. Land-cover and terrain morphology also affect the performance of filtering methods used to classify LiDAR 'ground' returns used to generate bare-earth DEMs (Aguilar et al., 2010). Identifying these possible sources of LiDAR error is important so that their influence on the overall data quality can be accounted for.

2 Existing standards used for LiDAR error

The quality of LiDAR is referred to as accuracy; 'a measurement is said to be more accurate when it offers a smaller measurement error' (JCGM, 2008: 21). We refer to LiDAR accuracy as 'error'. The National Digital Elevation Program (NDEP, 2004) and American Society of Photogrammetry and Remote Sensing (ASPRS, 2004) do not require horizontal (*xy*) error testing of elevation data. They note that this is because the topography may lack fine-scale terrain surface features required for horizontal testing, or the resolution of the elevation data is too coarse. However, NDEP (2004) documents that for high-resolution elevation data such as LiDAR, or in some cases IfSAR, where fine-scale terrain features (e.g. narrow stream junctions, small mounds) are identifiable, it is appropriate for data providers to test the horizontal error. Although the estimated horizontal error is important, the quality of LiDAR is primarily specified by the vertical error (ASPRS, 2004; NDEP, 2004). Therefore, studies address vertical error in SLR vulnerability mapping (Cooper et al., 2012; Gesch, 2009; Zhang, 2011). The vertical error of a DEM has the largest influence on delineating inundation zones (Zhang, 2011). For this reason, we focus on existing standards used to quantify LiDAR DEM vertical error.

Currently, there is no single standard established within the LiDAR community for assessing error. Generally, a combination of several existing standards is employed including: National Standards for Spatial Data Accuracy (NSSDA; FGDC, 1998), Federal Emergency Management Agency (FEMA, 2003), NDEP (2004), and ASPRS (2004). The NSSDA is the most commonly used (Congalton and Green, 2009) and preferred standard for assessing LiDAR error (Gesch et al., 2009). NSSDA uses statistical procedures for assessing and reporting error as an error statement, which originates from Greenwalt and Schultz (1962). An error statement indicates whether a product such as a LiDAR data set is reliable for a specific application such as SLR vulnerability mapping or whether the product should be used with caution.

Error is the difference between a measurement and a true value of the quantity being measured, which has two components: systematic errors and random errors (JCGM, 2008; Figure 1). In geodetic measurement, systematic errors are usually caused by flawed instrument calibration (Greenwalt and Schultz, 1962). Additionally, LiDAR systematic errors may originate from

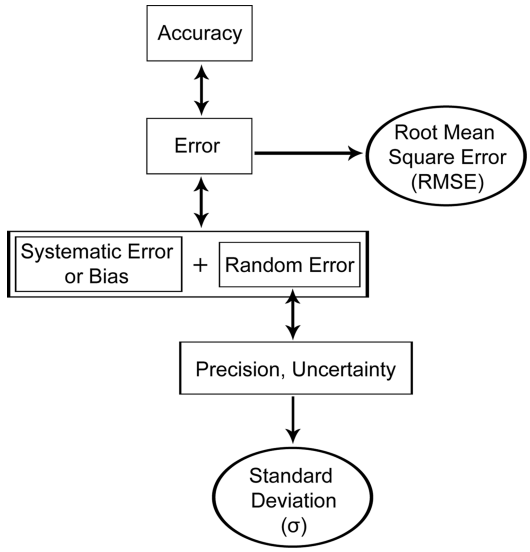

Figure 1. Interrelationship between error measurement terms and statistics. Double arrows denote measurement terms are interchangeable, single arrows denote links with statistics, and ovals denote statistics.

several sources, including the GPS constellation, IMU, and automated algorithms for classifying 'ground' returns (Hodgson et al., 2005). Bias is the estimate of a systematic error, and a systematic error (bias) can be controlled and characterized when the cause is known (JCGM, 2008). Correcting for bias is important because the probability that a random error will not exceed a certain magnitude is understood from a normal distribution with zero bias (Greenwalt and Schultz, 1962). A precision index is used to demonstrate the dispersal of errors about a mean of zero and to indicate the error at different probabilities (Greenwalt and Schultz, 1962). Precision is expressed numerically by measures of imprecision, which is usually the standard deviation (hereinafter denoted by σ; see Figure 1) (JCGM, 2008). Greenwalt and Schultz (1962) note that σ (Table 1) is used to compute a linear error at different probabilities:

$$\text{Greenwalt and Schultz linear error} = Z(\sigma) \quad (1)$$

where Z is the standard normal variable (Z-value) of the Z distribution at the desired probability level. In replacing the Z-value with the standard normal variable at the desired 95th probability level, an error statement may read '95% of all vertical errors occur within the limits of $\pm 1.96(\sigma)$'. The NSSDA measures error using RMSE (Table 1). The RMSE is the square root of the mean squared differences between the sample z values (vertical positions) of a geospatial data set and the z values of the same locations derived from an independent source of higher accuracy (FGDC, 1998). NSSDA cites Greenwalt and Schultz (1962) where 'if vertical error is normally distributed, the factor 1.96 is applied to compute the linear error at the 95% confidence level' (FGDC, 1998: 11). The NSSDA statistic for reporting error:

$$\text{NSSDA linear error} = 1.96(\text{RMSE}) \quad (2)$$

Congalton and Green (2009) point out that the NSSDA equation misinterprets the Greenwalt and Schultz (1962) equation by applying the RMSE in place of the σ. In fact, the validity of NSSDA linear error is based on two assumptions: (1) errors follow a normal distribution so that it is appropriate to use the standard normal variable of 1.96; (2) the data have a zero bias so that it is appropriate to use the RMSE instead of the σ (i.e. RMSE is equivalent to σ; see Figure 1 for the linkage and difference between RMSE and σ). When errors are not normally distributed, NDEP (2004) and ASPRS (2004) recommend using the 95th percentile method. The reliability of these statistics become increasingly important when used to address uncertainty in SLR vulnerability mapping.

3 Mapping vertical uncertainty

A number of studies acknowledge LiDAR uncertainty when mapping the inundation extent of SLR (Cooper et al., 2012; Gesch, 2009; Mitsova et al., 2012; NOAA, 2010b). In reality, many factors contribute quantifiable

Table 1. Equations for calculating standard deviation and root mean square error (RMSE).

Greenwalt and Schultz (1962)		NSSDA (FGDC, 1998)	
Standard deviation (σ)	$\sigma = \sqrt{\sum (Z_{data,i} - \bar{Z}_{data})^2 / n - 1}$ where: $Z_{data,i}$ = a value of the i^{th} sample chosen from the population; $\bar{Z}_{data}$ = estimated mean from sample; n = number of samples	Root mean square error (RMSE)	$RMSE = \sqrt{\sum (Z_{data,i} - Z_{check,i})^2 / n}$ where: $Z_{data,i}$ = elevation value of the i^{th} checkpoint in the geospatial data set; $Z_{check,i}$ = elevation value of the ith checkpoint in the independent source; n = number of points

sources of vertical uncertainty in vulnerability mapping, e.g. future SLR estimates, tidal datum models, vertical datum transformations, and LiDAR. NRC (2007) and Gesch (2009) document the principal criterion for a reliable SLR inundation boundary delineation is the quality of the input elevation data. LiDAR uncertainty passes on to the reliability of the SLR maps and analysis of potential impacts (Gesch et al., 2009).

Uncertainty is a parameter (e.g. σ or multiple of it) characterizing the dispersion of values within which the quantity being measured is situated within a stated level of confidence (JCGM, 2008). In other words, a common measure of uncertainty is σ, which should not be confused with RMSE. RMSE is a measure of uncertainty only when it is equal to σ. A tendency to cause confusion in SLR mapping is that the quality of the LiDAR data may refer to a measure of uncertainty denoted by σ, RMSE (most commonly reported; see Table 2), or NSSDA linear error.

A probabilistic inundation mapping approach by Merwade et al. (2008) demonstrates that the known vertical uncertainties (e.g. σ of SLR estimates and LiDAR) can be combined to delineate a zone of uncertainty around the inundation boundary. Gesch (2009) and Cooper et al. (2012) took a similar approach, in which the zone of uncertainty was defined by the NSSDA linear error and mapped above the inundation boundary. The purpose of this technique is to illustrate that the statistically related inundation bounds may fall anywhere within the zone determined by the LiDAR uncertainty (Gesch, 2009). The approach used by the National Oceanic and Atmospheric Administration's (NOAA) Coastal Services Center's (CSC) SLR mapping visualization tool and Mitsova et al. (2012) combine the vertical uncertainties associated with LiDAR and VDatum transformations. The purpose of this method is to map areas of high (e.g. 80%) and low (e.g. 20%) confidence using a modified standard-score equation:

$$\text{Standard} - \text{Score}_{(\text{grid cell})} = \frac{\text{SLR scenario} - \text{Elevation}_{(\text{grid cell})}}{\sigma_{(\text{RMSE and VDatum transformation})}} \quad (3)$$

where the $\sigma_{(\text{RMSE and VDatum transformation})}$ is represented by a single value calculated by summing in quadrature (Marcy et al., 2011; NOAA, 2010b). They note that major differences from Gesch (2009) include the use of a cumulative percentage in describing uncertainty (one tail versus two tail), and mapping the confidence interval both above and below the inundation extent. Unfortunately, many workers' attempt to reduce uncertainty is complicated by the absence of a LiDAR error standard.

4 Assuming a normal distribution with zero bias is sometimes violated

A significant barrier for SLR analysis using LiDAR is the lack of a comprehensive error

Table 2. Overview of LiDAR vertical error and relevant attributes in peer-reviewed SLR vulnerability mapping case studies. DEM = digital elevation model; SLR = sea-level rise; RMSE = root mean square error; N/A = not available.

Study	Geographic location	Sector	Point spacing (m)	DEM resolution (m)	SLR scenarios mapped (m)	RMSE (cm)
Webster et al., 2004	Prince Edward Island, Canada	Human	$\leq$3	2	0.10 increments up to 4	30
Webster et al., 2006	New Brunswick, Canada	Human and natural	0.6	1	0.5 and 0.7	16
			0.45			12
Poulter and Halpin, 2008	North Carolina, USA	N/A	N/A	6	0.025 increments up to 1.1	16
				15		20
Henman and Poulter, 2008	North Carolina, USA	Natural	N/A	15	0.35, 0.59, 0.82, and 1.38	25
Purvis et al., 2008	Somerset, England	Human	N/A	2 resampled to 50	0.48	10
Gesch, 2009	North Carolina, USA	Human	N/A	3	1	14
Chust et al., 2010	Gipuzkoa, Spain	Natural	N/A	1	0.49	15
Zhang, 2011	South Florida, USA	Human and natural	1.5	5	0.5, 1, 1.5	15
Zhang et al., 2011	Florida Keys, USA	Human	1.3	5	0.15 increments up to 5.1	9 and 15
Mitsova et al., 2012	Southeast Florida, USA	Human	N/A	N/A	0.23	N/A
Cooper et al., 2012	Maui Island, Hawai'i, USA	Human and natural	1.3	2	0.75 and 1.9	20
			2			16
Rotzoll and Fletcher, 2013	Honolulu, Hawai'i, USA	Human	N/A	1	0.33 increments up to 1 m	N/A

standard that addresses all potential sources of LiDAR error. Most commonly, the NSSDA linear error is applied as a single measure across the entire DEM. The major limitation is that it requires errors to follow a normal distribution with zero bias. Unfortunately, LiDAR errors are sometimes biased (e.g. Adams and Chandler, 2002; Aguilar and Mills, 2008; Hodgson et al., 2005). The lack of a standard method of describing LiDAR error provokes inconsistent and misleading reporting of uncertainty and error.

For example, in a LiDAR quality assessment report for the San Francisco Bay area (NOAA, 2011; Table 3), the NSSDA linear error is calculated for the land-cover category of open terrain (i.e. grass, sand, rocks, and dirt) where errors are assumed to follow a normal distribution with zero bias. Although the small skewness (which does not exceed ± 0.5) indicates that the errors for open terrain follow a normal distribution, they have a negative systematic bias. Therefore, replacing the σ with the RMSE to calculate the NSSDA linear error is invalid. The current practice of addressing LiDAR uncertainty in SLR mapping assumes that vertical errors follow a normal distribution with zero bias, which is

Table 3. LiDAR vertical error descriptive statistics for San Francisco Bay. RMSE = root mean square error; σ = standard deviation; no. of points = number of survey checkpoints. Modified from NOAA (2011).

Land-cover category	RMSE (cm)	Mean (cm)	Median (cm)	Skew	σ (cm)	No. of points	NSSDA Linear error	NDEP/ASPRS 95th percentile
Consolidated	4.7	0.0	–0.3	3.447	4.7	60		6.2 cm
Open terrain	**2.6**	**–1.3**	–0.9	**–0.207**	**2.3**	20	5.1 cm	5.3 cm
Marsh	7.2	2.5	0.4	2.485	7.0	20		15.4 cm
Urban	2.5	–1.0	–0.8	–0.556	2.3	20		4.7 cm

sometimes violated, as demonstrated above. Using this example of the San Francisco Bay LiDAR data set, the inundated area would be less reliable due to an incorrectly defined representation of map error (see Figure 2). The approach used by the NOAA CSC would also be less reliable because it 'assumes that the RMSE is analogous to the σ (i.e. the data are not biased), which allows for the generation for a type of Z-score or "standard score" from the data' (Marcy et al., 2011: 481; NOAA, 2010b: 3). Using the approaches outlined by Gesch (2009) and NOAA (2010b), one may overestimate the uncertainty of potential inundation areas because the RMSE is generally larger than the σ. The LiDAR elevation bias will further complicate the SLR mapping because LiDAR with a systematic positive bias will overestimate the land surface (e.g. Kraus and Pfeifer, 1998; Schmid et al., 2011), thus underestimating potential inundation. Likewise, LiDAR with a systematic negative bias will underestimate the land surface (e.g. Adams and Chandler, 2002; Hodgson et al., 2005), thus overestimating potential inundation. SLR vulnerability mapping calls for a comprehensive LiDAR error standard that considers these critical issues while addressing all potential sources of error.

IV Discrepancies between vertical datums

1 Vertical datums

Mapping SLR requires a basic understanding of the three major classes of vertical datums used to reference LiDAR: ellipsoidal, orthometric, and tidal datums (e.g. Gesch et al., 2009; Webster et al., 2004; see Figure 3). Normally, LiDAR data are first collected and referenced to an ellipsoidal datum (e.g. World Geodetic System of 1984), a smooth geometric surface with origin at Earth's mass center. LiDAR ellipsoidal elevations are transformed to orthometric elevations using a geoid model (e.g. Geoid 12), an equipotential surface defined by Earth's gravity field with one or more tide stations used as control points. The zero contour of a geoid model approximates the global MSL shoreline used for measuring orthometric elevations (NOAA, 2001). LiDAR orthometric elevations are commonly referenced to an orthometric datum such as the North American Vertical Datum of 1988 (NAVD 88) used in the continental USA. The zero contour of any orthometric datum does not equal the value of MSL defined by a tidal datum (e.g. Gesch et al., 2009; NOAA, 2010b). Tidal datums are defined by a certain phase of the tide at a fixed tide station location (NOAA, 2001). MSL tidal datum is the average of the mean sea-level elevations of each tidal day, and Mean Higher High Water (MHHW) tidal datum is the average of the mean higher high water elevations of each tidal day, both observed over a National Tidal Datum Epoch (NTDE) of 19 years (currently 1983–2001 for the USA; NOAA, 2003). MHHW is selected as the datum to map SLR inundation because it represents the modern highest high water mark where land is inundated daily. Discrepancies between orthometric and tidal datums can be significant, e.g. the difference

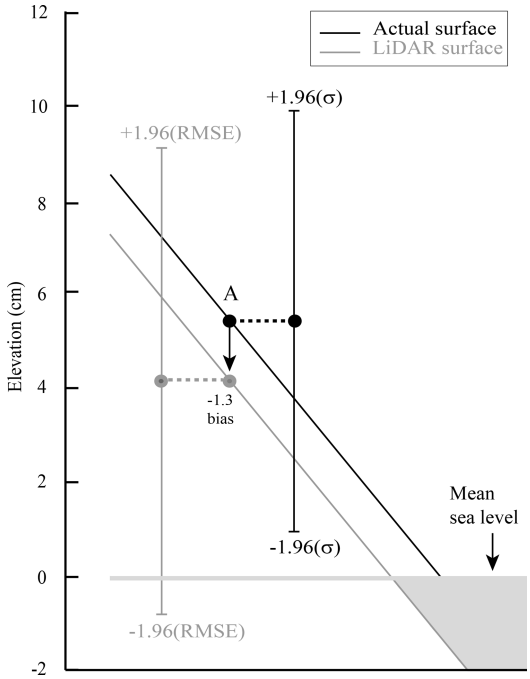

Figure 2. Applying the values from Table 3, the effect of using the root mean square error (RMSE) when LiDAR are negatively biased compared with using the standard deviation (σ) when LiDAR are not biased. For example, location A will be mistakenly labeled as 'inundated' if (1) we assume the LiDAR surface has no bias although actually there is –1.3 cm bias, and (2) RMSE is used in replacement of σ to calculate NSSDA linear error. Note: when LiDAR are not biased, the RMSE is equal to the σ.

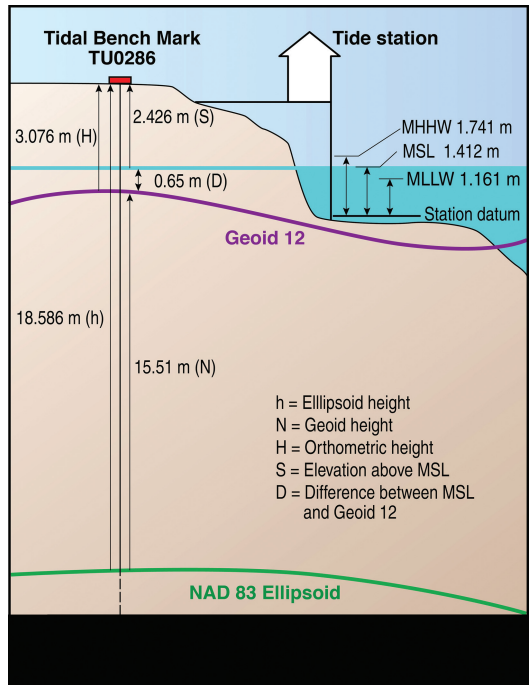

Figure 3. Example illustration demonstrating differences between datums using the Honolulu Tide Station. Ellipsoidal datum of NAD 83 = North American Datum of 1983. Tidal datums of MHHW = Mean Higher High Water; MSL = Mean Sea Level; MLLW = Mean Lower Low Water (1983–2001 epoch). Station datum is the zero reference for measuring tidal datums.

between NAVD 88 and MSL often exceeds 1 m along the US West Coast (Gesch et al., 2009). SLR vulnerability mapping requires an understanding of the orthometric datum to which LiDAR elevations are referenced, MSL and MHHW defined by a tidal datum to evaluate whether a vertical transformation is needed.

Here, we attempt to illustrate the importance of vertical datum transformations and consider existing approaches used to address this issue. A SLR scenario of 32 cm (Rignot et al., 2011) and the location of a National Geodetic Survey (NGS) and National Ocean Service (NOS; http://tidesandcurrents.noaa.gov) primary tidal benchmark near the Honolulu Tide Station are examined (Figure 3). Increasing sea level to 32 cm above Geoid 12 at this location results in mapping areas already inundated at MSL (1983–2001 epoch) because Geoid 12 is 65 cm below MSL. To correct this discrepancy, the relationship of the geoid and MSL must be established, which only can be determined at a tidal benchmark (NOAA, 2008). Many workers use tidal benchmarks to establish relations between orthometric elevations and tidal datums (e.g. Chust et al., 2010; Cooper et al., 2012; Webster et al., 2004). NOAA (2010c) offers a technique where the difference between Geoid 12 and MSL (+65 cm) is assumed as a

constant offset (i.e. geoid separation from MSL) that is extended inland by extrapolation for a transformation to MSL. However, increasing sea level to 32 cm above MSL results in mapping areas already inundated at MHHW (1983–2001 epoch) because MSL is 32.9 cm below MHHW. To map SLR relative to MHHW, a second transformation between tidal datums is needed. Following NOAA (2010c), the difference between MSL and MHHW (+32.9 cm) is assumed as a constant offset that is extrapolated inland for a conversion to MHHW. Ultimately, increasing sea level to 32 cm above the MHHW shoreline distinguishes between the modern higher high watermark and the added SLR increment. It is noted by Gesch et al. (2009) that descriptive statistics (e.g. mean, σ) on the variability of datum transformations needs to be documented. Their technique can be applied to any coastal region around the world where the relationship between a geoid model and tidal datums can be determined at tidal benchmarks. This is applicable when the geoid is of high enough resolution to characterize the coastline. For the conterminous USA, discrepancies between vertical datums may be addressed using VDatum.

2 VDatum

A vertical datum transformation tool, VDatum (http://vdatum.noaa.gov), was developed for the conterminous USA by NOAA NOS and NGS to transform elevation data among approximately 30 vertical reference systems within the three major classes (Parker, 2002). VDatum uses Topography of the Sea Surface (TSS) to convert between NAVD 88 and MSL (e.g. Myers et al., 2005). The TSS is generated for a region by interpolating the difference between MSL (observed at NOS tidal benchmarks) and NAVD 88 elevations (e.g. Hess et al., 2005). VDatum uses a hydrodynamic model called ADvanced CIRCulation model (ADCIRC) to simulate tidal datums of a region (e.g. Hess et al., 2005). A spatial interpolation technique called Tidal Constituent and Residual Interpolation (TCARI; Hess, 2002) is used to calibrate the hydrodynamic modeled tidal datums with observed tidal datums over a 19-year epoch at nearby tide stations (Parker et al., 2003). The corrected modeled tidal datums are interpolated onto a spatial variable resolution grid of sea surface elevations used for converting between tidal datums (Myers et al., 2005).

VDatum is the industry standard in the USA for transforming LiDAR elevations between vertical datums. Here we provide a preliminary assessment of vertical uncertainties in VDatum, as found in NOAA (2012). The Delaware Bay region is used as an example when transforming values from the International Terrestrial Reference Frame of year XX (ITRFxx)-to-MHHW that is typical for a SLR vulnerability mapping project (Figure 4). The σ is used to quantify uncertainties between two groups in VDatum: source data (e.g. North American Datum of 1983 (NAD 83), NAVD 88, MSL, and MHHW) and transformations (e.g. ITRFxx-to-NAD 83, NAD 83-to-NAVD 88, NAVD 88-to-MSL, and MSL-to-MHHW). For individual uncertainties of source data, VDatum considers a constant σ of 2 cm for NAD 83, and a constant σ of 5 cm for NAVD 88 nationwide (Zilkoski et al., 1992); additionally, MSL and MHHW uncertainties throughout the Delaware Bay region are calculated as having a single σ of 1.3 cm (NOAA, 2012). It is assumed that the individual uncertainties are independent (the value of one measurement does not affect the value of the other measurement) and randomly distributed (follow a normal distribution), so that all uncertainties may be represented by a single value calculated by summing in quadrature. The total uncertainty of all source data in the Delaware Bay region is: $\sqrt{2^2 + 5^2 + 1.3^2 + 1.3^2} = 5.7\text{cm}$. For individual uncertainties of transformations, ITRFxx-to-NAD 83 σ is 2 cm, NAD 83-to-NAVD 88 σ is 5 cm, NAVD 88-to-MSL (TSS transformation uncertainty) σ is 8.6 cm; additionally, MSL-to-

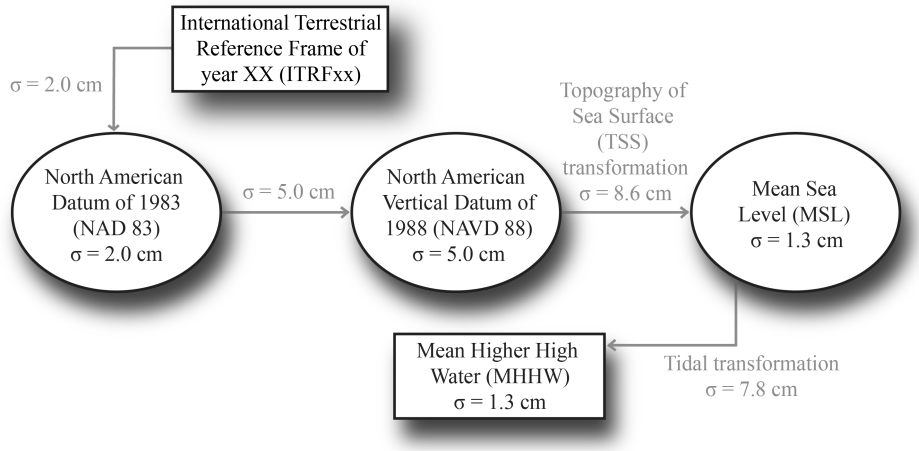

Figure 4. VDatum errors calculated as standard deviation values (σ) for Delaware Bay region from NOAA (2012). Arrows denote transformation processes, ovals denote core datums, and rectangles denote individual vertical datums.

MHHW (tidal transformation accuracy) σ is 7.8 cm (NOAA, 2012). The total uncertainty of all transformations in the Delaware Bay region is: $\sqrt{2^2 + 5^2 + 8.6^2 + 7.8^2} = 12.8\text{cm}$. The total uncertainty of the source data and transformations can be calculated by summing in quadrature as the Maximum Cumulative Uncertainty (MCU) $= \sqrt{5.7^2 + 12.8^2} = 14\text{cm}$. The MCU can be derived for any region in the conterminous USA following NOAA (2012), and the calculation and transformation details can be documented in SLR studies employing VDatum. These transformation errors are used in the NOAA CSC's SLR mapping visualization tool for mapping inundation uncertainty (http://www.csc.noaa.gov/slr/viewer). However, for short-term SLR planning targets (e.g. 32 cm by year 2050), current VDatum errors may complicate generating accurate inundation maps referenced to MHHW.

V Mapping minimum statistically significant SLR scenarios

Producing vulnerability maps useful for planning involves determining the minimum SLR scenario to map. The minimum statistically significant SLR increment is a function of the vertical error of the elevation data (Gesch et al., 2009). For example, Zhang et al. (2011) mapped SLR increments relative to the RMSE. The NRC (2007) recommends that LiDAR quality meet a minimum RMSE of 9.25 cm for coastal areas vulnerable to coastal hazards. Gesch et al. (2009) note that the minimum SLR increment supported by such a data set is the NSSDA linear error ($1.96 \times 9.25 = 18.1\text{cm}$); however, the reliability of the mapped vulnerable areas are low because the SLR increment is equal to the LiDAR error. The quality of a vulnerability map is increased when the LiDAR error is at least twice as certain as the SLR increment (Gesch et al., 2009), which is referred to as a 'rule of thumb' (NOAA, 2010c: 103). Increasing the NSSDA linear error of 18.1 cm by the factor 2 results in more reliable SLR vulnerability mapping of 36.3 cm increments ($2 \times 18.1 = 36.3\text{cm}$). Following these guidelines by Gesch et al. (2009) and Gesch (2012), we note that SLR vulnerability mapping of short-term planning targets of 32 cm and below requires a RMSE of 8.2 cm and better if bias is zero. However, in

addition to LiDAR error, choosing the minimum statistically significant SLR scenario to map is also a function of vertical datum transformation error.

Here we assume that the individual LiDAR and VDatum uncertainties are independent and normally distributed so that the total uncertainty can be calculated. For example, we consider the ITRFxx-to-MHHW transformation using VDatum MCU of 14 cm for the Delaware Bay (section IV), and the NRC (2007) minimally required RMSE of 9.25 cm, and calculate the LiDAR and VDatum total error: $\sqrt{9.25^2 + 14^2} = 16.77$cm. Increasing the total uncertainty of 16.77 cm by the factor 1.96 results in a minimum SLR scenario of 32.87 cm ($1.96 \times 16.77 = 32.87$cm); however, the reliability of the mapped vulnerable areas is low because the SLR increment is equal to the LiDAR and VDatum total error. The quality of a vulnerability map is increased when the LiDAR and vertical datum transformation total uncertainty is at least twice as certain as the SLR increment. Increasing the total uncertainty by the factor 2 results in mapping minimum statistically significant SLR increments of 65.7 cm ($32.87 \times 2 = 65.7$cm). This example demonstrates that it is difficult to generate an accurate inundation map using short-term SLR planning targets (e.g. 32 cm by year 2050) based on current LiDAR and VDatum errors.

VI LiDAR processing for DEM generation and bias correction

Some important issues in LiDAR DEM generation include interpolation algorithms, DEM resolution, and filtering or classification algorithms (Liu, 2008). The most complicated, yet fundamental first step for LiDAR DEM generation is the processing of the LiDAR point cloud (points defined by *xyz* in a coordinate system) into classified 'ground' and 'non-ground' returns (e.g. vegetation or buildings; Chen et al., 2007; Liu, 2008; Webster et al., 2006). SLR vulnerability mapping requires quality DEMs derived from LiDAR returns classified as bare earth or 'ground'. LiDAR providers use proprietary algorithms to classify and remove 'non-ground' returns (Hodgson and Bresnahan, 2004; Schmid et al., 2011). Most algorithms are centered on the difference between geometric characteristics of the LiDAR point cloud for terrain and non-terrain features (Sithole and Vosselman, 2004; Zhang and Whitman, 2005), yet these processes are not completely effective; there is still room for improvement (Liu, 2008). LiDAR providers usually perform manual inspection by a human operator, which tends to be labor intensive but dramatically improves the quality of the classification results (Hodgson et al., 2005). Unfortunately, not all LiDAR providers perform classification or remove returns over vegetated areas successfully (Cooper et al., 2012; Hodgson et al., 2005; Schmid et al., 2011).

It is cautioned that end-users should not assume any given LiDAR data set represents the surface (e.g. bare earth) intended for their application (Schmid et al., 2011). Few studies critically accept LiDAR point data from the provider to assess the quality. One method used to improve the bare-earth file is to fine-tune classification results of 'ground' returns. For example, Webster et al. (2004, 2006) note that the filtering algorithms used a threshold filter where 'non-ground' returns were classified based on abrupt elevation changes relative to their neighbors, which caused LiDAR returns on irregularly high elevations such as wharf edges, seawalls, cliffs and coastal dunes to be incorrectly classified as 'non-ground'. They manually inspected the 'non-ground' return file and reclassified the LiDAR returns on top of these coastal terrain features as 'ground' to include in a newly generated DEM. Thus, it is important LiDAR providers make available to end-users both 'ground' and 'non-ground' return files. Cooper et al. (2012) manually inspected the 'ground' return file overlain with orthophotos and identified LiDAR returns on top of vegetation surrounding a

freshwater marsh that should have been classified as 'non-ground'. They reclassified the LiDAR returns over vegetation as 'non-ground' to fine-tune classification in the 'ground' return file; otherwise, they found that a DEM generated from the original LiDAR 'ground' return file underestimated the extent of potential SLR. An advantage to filtering is the possibility to detect bare-earth points while maintaining point density (Schmid et al., 2011). However, a disadvantage is that not all end-users have available the required software to reclassify LiDAR data.

In the absence of filtering software, Schmid et al. (2011) demonstrate another technique for end-users to improve estimates of ground elevations in coastal marshes: minimum bin methods (selects lowest elevation point in a user-defined grid resolution to represent each grid cell in the output raster). Problems encountered in the bare-earth file included coastal marsh vegetation (>1 m in height) incorrectly classified as 'ground'. They document that although the minimum bin method removes more points resulting in a coarser resolution DEM, this is manageable in coastal marshes where topographic variations are limited. After the bare-earth file is inspected for quality and used to generate a DEM, a quantitative assessment should be employed to correct any bias.

End-users typically identify bias by comparing LiDAR DEM elevations with independently collected Ground Control Points (GCPs) to calculate mean vertical error (i.e. bias), σ, and RMSE. Vegetation is known to cause a positive bias (e.g. Hladik and Albers, 2012; Schmid et al., 2011). For coastal marsh vegetation areas, Schmid et al. (2011) report that vertical errors for the non-minimum bin DEM (2 m resolution) are more biased with a higher RMSE than when compared to the minimum bin DEM (5 m resolution) using GCPs. However, the minimum bin method may underestimate (i.e. negative bias) upland areas with steeper slopes and tidal streams. To correct this negative bias and reduce the RMSE, an adjustment was made by increasing DEM values (>1 m) in upland areas by the mean error (bias). Hladik and Alber (2012) developed a species-specific correction factor quantified from GCPs as the mean error for each coastal marsh vegetation type. They found that the LiDAR DEM overestimated (i.e. positive bias) each marsh cover type, so the species-specific correction factor was subtracted from each marsh cover type in the DEM to correct for bias and reduce the RMSE. Cooper et al. (2012) took a different approach by calibrating one LiDAR DEM with tidal benchmarks, which was used to compare elevations of a second LiDAR DEM where tidal benchmarks were absent. They found that the second LiDAR DEM overestimated the land surface creating a positive bias, so an adjustment was made by decreasing the second DEM by the mean error. After the quality of the LiDAR filtering results is examined for DEM generation, and any bias corrected, often the next step is to model SLR inundation.

VII SLR inundation modeling

LiDAR DEMs are integrated into a Geographic Information System (GIS) to identify grid cells with elevations at or below a SLR planning target. Known as a 'bathtub' approach, this is an essential first step that results in identifying vulnerable grid cells that are both disconnected from and connected to ocean waters. It is argued that this simple practice is inadequate to modeling inundation because it is assumed that only areas connected to the ocean will be flooded (Poulter and Halpin, 2008). On the other hand, it is assumed that areas disconnected from the ocean will also experience groundwater inundation (Cooper et al., 2012; Reynolds et al., 2012; Rotzoll and Fletcher, 2013). Three techniques are used to identify areas submerged.

The first approach converts vulnerable grid cells to polygons and uses visual determination and manual selection of polygons open to the ocean. A benefit of this technique is that it helps to visually identify features in the LiDAR DEM

that obstruct hydraulic flow. For example, Webster et al. (2006) found that bridges and raised roadbeds in the DEM blocked stream channels causing some polygons to be cut off from direct marine inundation. They modified the DEM by 'notching' bridges and roadbeds to correct flow through low-lying stream channels. In Webster et al. (2004), engineers were also consulted to better assist in the identification of which areas upstream from culverts should be included in the manual selection. Chust et al. (2010) reasoned that some polygons, not open to direct marine inundation, should also be selected in order to locate potentially vulnerable crops preserved by walls. A limitation to this approach, similar to the process of a human operator manually classifying 'ground' returns, is that it tends to be labor intensive.

A second technique uses hydrodynamic modeling to identify grid cells as vulnerable to inundation. Purvis et al. (2008) modeled the flow between each direction of a cell using a two-dimensional hydrodynamic model to simulate extreme flooding events coupled with SLR. A restriction to this approach is that it requires intense computation time, in which the horizontal resolution of the LiDAR DEM was resampled from 2 to 50 m. Zhang (2011) notes that low LiDAR DEM resolutions (e.g. 30 m) have little effect when modeling inundation on regions at the magnitude of hundreds of square kilometers, yet high resolutions (e.g. 5 m) are essential for SLR decision-making involving individual properties at risk. Therefore, the use of hydrodynamic modeling, as in the case of Purvis et al. (2008), may be practical for regions of considerable extent.

The third approach (which is actually an automated version of the first approach) models direct marine inundation based on the assumptions of hydrologic connectivity. Poulter and Halpin (2008) reason that hydrologic connectivity effectively constrains the spread of SLR by specifying whether a grid cell is directly submerged. Hydrologic connectivity is modeled using the 4 sides of a grid cell in the cardinal directions (Poulter and Halpin, 2008; Zhang et al., 2011), and the 8 sides of a grid cell in the diagonal and cardinal directions (e.g. Cooper et al., 2012; Gesch, 2009; Poulter and Halpin, 2008). A drawback to this technique is that the 4-side connectivity rule may underestimate potential impacts, and conversely, the 8-side connectivity rule may overestimate potential impacts (Poulter and Halpin, 2008; see Figure 5). The 8-side connectivity assumption may be the more conservative approach to use for planning.

Planners need maps that illustrate both direct marine inundation and groundwater inundation (reduced drainage coupled with higher water tables). Modeling direct marine inundation alone will underestimate potential impacts because low-lying areas disconnected from ocean waters will also experience some form of flooding under SLR. Until recently, the impact of SLR through groundwater inundation was largely unknown (Rotzoll and Fletcher, 2013). Higher groundwater levels have the potential to submerge underground infrastructure, flood basements, reduce overland peak discharge (Bjerklie et al., 2012) and create inland areas characterized by standing pools of brackish water (Rotzoll and Fletcher, 2013). One useful approach is to symbolize areas connected to the ocean differently from areas not connected to the ocean (Cooper et al., 2012; Marcy et al., 2011; Zhang et al., 2011). Rotzoll and Fletcher (2013) found that the latter reveals widespread flooding of inland areas before direct marine inundation, which is also identified in maps by Cooper et al. (2012). Reynolds et al. (2012) identify grid cells vulnerable to groundwater inundation by areas connected to an inland lake. Following Bjerklie et al. (2012), they predicted that a 1 m rise in sea level would be equivalent to a 1 m rise in the groundwater table causing the lake to expand. Grid cells vulnerable to both direct marine inundation and groundwater inundation are often converted to polygons to create vectorized SLR hazard data layers to be used in spatial analysis.

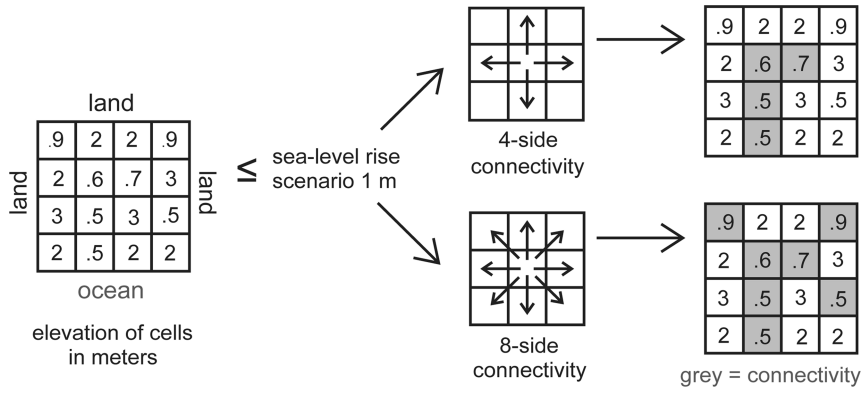

Figure 5. Demonstration of fewer cells connected using the 4-side approach compared to many cells connected using the 8-side approach.

VIII Vulnerability by sector

Spatial analysis in a GIS is the preferred technique for evaluating the potential impacts of SLR on existing coastal systems. For example, land loss due to the impacts of SLR on higher water tables was evaluated by compiling existing coastal groundwater data to estimate the water table at MHHW coupled with SLR (Rotzoll and Fletcher, 2013). Land loss due to the effect of SLR on coastal erosion was calculated using the Bruun rule (Bruun, 1988; Chust et al., 2010). Zhang et al. (2013) determined the storm surge flooding with SLR using a numerical model by considering the non-linear interaction between SLR and storm surge. Reynolds et al. (2012) modeled inundation due to wave-driven water levels (wave set-up + wave run-up) combined with SLR. As we begin to understand other physical effects of SLR, we need to incorporate these effects into SLR vulnerability mapping.

The biophysical impacts of SLR on existing natural systems are often examined (Table 2) by overlaying the SLR hazard layers with other data layers that characterize natural coastal systems. Chust et al. (2010) used coastal habitat data layers such as sandy beaches, wetlands, and vegetated dunes to estimate potential habitat loss and found that environmental change threatens coastal biodiversity, especially among sandy beach habitat. Change in wetlands (e.g. salt marshes) is a response of the relation of rising sea levels to tidal ranges, and SLR hazard layers were used to identify the extent of landward migration (Webster et al., 2006). In efforts to help managers protect endangered native water bird species habitat where additional wildlife conservation is anticipated, SLR hazard layers delineated potential wetland expansion as a result of reduced drainage coupled with rising water tables and potential wetland loss (where wetlands open up to the ocean; Cooper et al., 2012). Adaptation strategies to groundwater inundation will be difficult when high tides coincide with rainfall, thus requiring more complex planning tools than direct marine inundation (Rotzoll and Fletcher, 2013). Henman and Poulter (2008) combined peat soils data layers and the National Land Cover Dataset (NLCD; developed by the US Geological Survey c. 2001; Homer et al., 2004) to define the area of peat and vegetation type loss. They concluded that higher seas on freshwater coastal peatlands might contribute to a larger amount of carbon to aquatic habitats and the atmosphere than previously recognized.

Studies also assess the economic impacts of SLR defined by damage costs (Table 2). However, adaptation costs such as beach and wetland

nourishment, and saltwater intrusion barriers, are not assessed. Overlay of SLR and associated storm surge hazard layers with land-use data layers derived from the Land Cover Map of Great Britain 2000 (Fuller et al., 1994) provided estimates of the costs of potential land loss (Purvis et al., 2008). Up-to-date land parcel data layers provided by the respective counties were intersected with SLR hazard layers to measure costs of potential property loss (Cooper et al., 2012; Zhang et al., 2011) and building loss (Cooper et al., 2012) based on the percentage of each parcel inundated. Zhang (2011) used a different approach to evaluate the costs of property loss where a land parcel is assumed inundated if its centroid is within the SLR inundation layer. He found problems in the land parcel data such as duplicate parcel identifications that needed correction. This is a good indicator that the quality of the data used to characterize vulnerabilities should be examined, and perhaps improved, before use in SLR vulnerability assessment. Webster et al. (2004) conclude that estimating the potential costs of inundation on critical infrastructure, properties, businesses, and heritage sites results in effective planning and prompt adaptation of new procedures for building permits.

Evaluating the potential social impacts is defined by the amount of actual and anticipated populations subject to SLR, which tends to be challenging due to population numbers not being uniform throughout census block layers. Zhang (2011) and Zhang et al. (2011) assumed that a 2000 census block was inundated based on the centroid approach discussed above. Zhang et al. (2011) note that the population impacted could also be approximated based on the percentage of the census block submerged (if the census blocks are not too large in size). However, census blocks tend to be much larger in size (at the order of kilometers) compared to land parcel data layers, thus reducing the practical use of census block data for fine-scale SLR mapping. On the other hand, Gesch et al. (2009) suggested the use of dasymetric mapping to improve analysis of vulnerable population and socio-economic data. Mitsova et al. (2012) used dasymetric mapping techniques to interpolate 2010 census block population numbers and county population projections to the smaller land parcel units. They confirm that this approach more effectively characterizes existing and future population distributions vulnerable to SLR.

IX Best practices in SLR vulnerability mapping

In their analysis of SLR vulnerability mapping for Maui, the authors implement many of the best practices discussed above (Cooper et al., 2012). They test a series of global SLR estimates for a long-term planning target, but where regional SLR estimates are available for short and long-term planning targets, we note that these should be included into analysis of future impacts. Additionally, the authors incorporate the LiDAR uncertainty into both the vulnerability maps and derived assessments of potential impacts. However, they make the same assumption that the data are normally distributed with zero bias. This problem stems from some LiDAR providers not following current available guidelines and not reporting descriptive statistics (e.g. RMSE, mean error or bias, σ, skewness), and, overall, the lack of a LiDAR error standard. Tidal benchmarks are used to calibrate LiDAR elevations with MSL tidal datum and descriptive statistics are reported. They present an approach to adjust for a statistically significant bias when working with more than one LiDAR data set for areas lacking tidal benchmarks (and VDatum). The quality of the LiDAR point data files is inspected before DEM generation, and SLR is mapped above MHHW. Areas vulnerable to marine and groundwater inundation are symbolized differently in the vulnerability maps and quantified separately in the derived estimates of potential impacts.

X Conclusions

The objective of this paper is to review current published practices in SLR vulnerability mapping to determine whether there are minimum criteria that LiDAR elevation data should meet when applied in SLR decision-making. The authors identify the following:

- Research is converging on a short-term planning target of 32 cm global SLR by 2050 and a long-term planning target of 1 m global SLR by 2100.
- The most commonly used guideline for reporting LiDAR error, NSSDA linear error, is based on two assumptions: (1) errors follow a normal distribution allowing use of the standard normal variable of 1.96; (2) data have a zero bias allowing use of the RMSE instead of the σ (i.e. the RMSE is equivalent to the σ).
- The deficiency of a standard method of describing all potential sources of LiDAR error provokes inconsistent and misleading reporting of uncertainty and error.
- The current practice of SLR mapping assumes that LiDAR vertical errors follow a normal distribution with zero bias, which is sometimes violated. End-users will benefit if LiDAR providers document descriptive statistics (e.g. RMSE, mean error or bias, σ, skewness).
- Mapping a minimum statistically significant SLR planning target of 32 cm is difficult to achieve based on current LiDAR and VDatum data sets.
- SLR vulnerability mapping often requires two datum conversions: (1) land datum to which LiDAR elevations are referenced to local tidal datum of MSL; (2) MSL to local tidal datum of MHHW.
- DEMs derived from LiDAR returns classified as bare earth or 'ground' is essential, yet not all LiDAR providers perform classification or remove returns over vegetated areas successfully.
- Planners need maps that illustrate both marine and groundwater inundation. Modeling direct marine inundation alone will underestimate potential impacts because low-lying areas disconnected from ocean waters will also experience flooding.

It is expected that this review will result in better practice of the use of LiDAR DEMs in SLR vulnerability mapping. The authors identify continuing research in areas of rectifying coastal DEMs with local tidal datums. New methodologies such as Monte Carlo may incorporate the many uncertainties in vulnerability mapping such as LiDAR data, vertical datum transformations, local tidal datums, future SLR estimates, groundwater table elevations, changing storm surges, wave overtopping, etc. New ways of communicating vulnerability may include using flow diagrams of which direction inundation would flow. Further research is needed in identifying the true relationship between bare-earth products and ground level. Additionally, new assessments of adaptation costs such as beach and wetland nourishment, and saltwater intrusion barriers may compliment the SLR vulnerability mapping.

Funding

This study was funded by a grant from the US Department of Interior, Pacific Islands Climate Change Cooperative (Honolulu, HI). We thank Ev Wingert, Reece Jones, Ed Carlson, Michael O. Garcia, Tiffany Anderson, and Julius R. Paulo. Data made available from NOAA NOS, and NGS.

References

Adams J and Chandler J (2002) Evaluation of lidar and medium scale photogrammetry for detecting soft-cliff coastal change. *The Photogrammetric Record* 17(99): 405–418.

Adger N (2006) Vulnerability. *Global Environmental Change* 16(3): 268–281.

Adger N, Hughes T, Folke C, et al. (2005) Social-ecological resilience to coastal disasters. *Science* 309(5737): 1036–1039.

Aguilar F and Mills J (2008) Accuracy assessment of lidar-derived digital elevation models. *The Photogrammetric Record* 23(122): 148–169.

Aguilar F, Mills J, Delgado J, et al. (2010) Modelling vertical error in lidar-derived digital elevation models. *ISPRS Journal of Photogrammetry and Remote Sensing* 65: 103–110.

American Society of Photogrammetry and Remote Sensing (ASPRS) (2004) ASPRS guidelines vertical accuracy reporting for lidar data (version 1.0). Report for the American Society for Photogrammetry and Remote Sensing Lidar Committee, 24 May.

Bjerklie D, Mullany J, Stone J, et al. (2012) Preliminary investigation of the effects of sea-level rise on groundwater levels in New Haven Connecticut. US Geological Survey Report no. 2012–1025.

Brock J and Purkis S (2009) The emerging role of lidar remote sensing in coastal research and resource management. *Journal of Coastal Research* 53: 1–5.

Brown I (2006) Modelling future landscape change on coastal floodplains using a rule-based GIS. *Environmental Modeling and Software* 21: 1479–1490.

Bruun P (1988) The Bruun rule of erosion by sea-level rise: A discussion of large-scale two- and three-dimensional usages. *Journal of Coastal Research* 4(4): 627–648.

Chen Q, Gong P, Baldocchi D, et al. (2007) Filtering airborne laser scanning data with morphological methods. *Photogrammetric Engineering and Remote Sensing* 73(2): 175–185.

Church J and White N (2006) A 20th century acceleration in global sea-level rise. *Geophysical Research Letters* 33: L01602.

Church J and White N (2011) Sea-level rise from the late 19th to the early 21st century. *Surveys in Geophysics* 32(4–5): 585–602.

Church J, Gregory J, White N, et al. (2011) Understanding and projecting sea level change. *Oceanography* 24(2): 130–143.

Chust G, Caballero A, Marcos M, et al. (2010) Regional scenarios of sea-level rise and impacts on Basque (Bay of Biscay) coastal habitats, throughout the 21st century. *Estuarine, Coastal and Shelf Science* 87(1): 113–124.

Congalton R and Green K (2009) *Assessing the Accuracy of Remotely Sensed Data: Principles and Practices*, second edition. Boca Raton, FL: Taylor and Francis.

Cooper H, Chen Q, Fletcher C, et al. (2012) Vulnerability assessment due to sea-level rise in Maui, Hawai'i using lidar remote sensing and GIS. *Climatic Change* 116(3–4): 547–563.

Coveney S and Fotheringham A (2011) The impact of DEM data source on prediction of flooding and erosion risk due to sea-level rise. *International Journal of Geographical Information Science* 23(7): 1191–1211.

Coveney S, Fotheringham A, Charlton M, et al. (2010) Dual-scale validation of medium-resolution coastal DEM with terrestrial lidar DSM and GPS. *Computer and Geosciences* 36(4): 489–499.

Dawson R, Hall J, Bates P, et al. (2005) Quantified analysis of the probability of flooding in the Thames Estuary under imaginable worst-case sea level rise scenarios. *International Journal of Water Resources Development* 21(4): 577–591.

Federal Emergency Management Agency (FEMA) (2003) Guidelines and specifications for flood hazard mapping partners. Available at: http://www.fema.gov/library/viewRecord.do?id=2206.

Federal Geographic Data Committee (FGDC) (1998) Geospatial positioning accuracy standards, Part 3: National Standard for Spatial Data Accuracy. US Geological Survey Report no. FGDC-STD-007.3-1998.

Fletcher CH (2009) Sea level by the end of the 21st century: A review. *Shore and Beach* 77(4): 4–12.

Florida Oceans and Florida Coastal Council (2010) Climate change and sea level rise in Florida: An update of the effects of climate change on Florida's ocean and coastal resources. Report. Tallahassee, FL: Florida Oceans and Florida Coastal Council.

Fuller RM, Groom GB, and Jones AR (1994) The land cover map of Great Britain: An automated classification of Landsat Thematic Mapper data. *Photogrammetric Engineering and Remote Sensing* 60: 553–562.

Gesch D (2009) Analysis of lidar elevation data for improved identification and delineation of lands vulnerable to sea-level rise. *Journal of Coastal Research* 53: 49–58.

Gesch D (2012) Elevation uncertainty in coastal inundation hazard assessments. In: Cheval S (ed.) *Natural Disasters*. Rijeka, Croatia: In Tech, 121–140.

Gesch D, Guitierrez B, and Gill S (2009) Coastal elevations. In: Titus J, Anderson E, Cahoon D, et al. (eds) *Coastal Sensitivity to Sea-Level Rise: A Focus on the Mid-Atlantic Region*. Washington, DC: US Government Printing Office, 25–42.

Greenwalt C and Shultz M (1962) Principles of error theory and cartographic applications. Report no. 96, February.

St Louis, MO: Aeronautical Chart and Information Center.

Henman J and Poulter B (2008) Inundation of freshwater peatlands by sea level rise: Uncertainty and potential carbon cycle feedbacks. *Journal of Geophysical Research* 113: G01011.

Hess K (2002) Spatial interpolation of tidal data in irregularly-shaped coastal regions by numerical solution of Laplace's Equation. *Estuarine, Coastal and Shelf Science* 54(2): 175–192.

Hess K, Spargo E, Wong A, et al. (2005) VDatum for central coastal North Carolina: Tidal datums, marine grids, and sea surface topography. Report no. NOS CS 21, December. Silver Spring, MD: National Oceanic and Atmospheric Administration.

Hinkel J and Klein R (2009) Integrating knowledge to assess coastal vulnerability to sea-level rise: The development of the DIVA tool. *Global Environmental Change* 19(3): 384–395.

Hinkel J, Nicholls R, Vafeidis A, et al. (2010) Assessing risk of and adaptation to sea-level rise in the European Union: An application of DIVA. *Mitigation and Adaptation Strategies for Global Change* 15(7): 703–719.

Hladik C and Alber M (2012) Accuracy assessment and correction of a lidar-derived salt marsh digital elevation model. *Remote Sensing of Environment* 121: 224–235.

Hodgson M and Bresnahan P (2004) Accuracy of airborne lidar-derived elevation: Empirical assessment and error budget. *Photogrammetric Engineering and Remote Sensing* 70(3): 331–339.

Hodgson M, Jenson J, Raber G, et al. (2005) An evaluation of lidar-derived elevation and terrain slope in leaf-off conditions. *Photogrammetric Engineering and Remote Sensing* 71(7): 817–823.

Homer C, Huang C, Yang L, et al. (2004) Development of a 2001 national land-cover database for the United States. *Photogrammetric Engineering and Remote Sensing* 70: 829–840.

Intergovernmental Panel on Climate Change (IPCC) (2007) *Climate Change 2007: The Physical Science Basis. Contribution of Working Group I to the Fourth Assessment Report of the Intergovernmental Panel on Climate Change*. Cambridge: Cambridge University Press.

Joint Committee for Guides in Metrology (JCGM) (2008) International vocabulary of metrology – basic and general concepts and associated terms (VIM). Working Group 2 of the Joint Committee for Guides in Metrology. Available at: www.bipm.org/utils/common/documents/jcgm/JCGM_200_2008.pdf.

Jevrejeva S, Moore J, and Grinsted A (2010) How will sea level respond to changes in natural anthropogenic forcings by 2100? *Geophysical Research Letters* 37: L07703.

Jevrejeva S, Moore J, and Grinsted A (2012) Sea level projections to AD2500 with a new generation of climate change scenarios. *Global and Planetary Change* 80–81: 14–20.

Kettle N (2012) Exposing compounding uncertainties in sea level rise assessments. *Journal of Coastal Research* 28(1): 161–173.

Kraus K and Pfeifer N (1998) Determination of terrain models in wooded areas with airborne laser scanner data. *ISPRS Journal of Photogrammetry and Remote Sensing* 53(4): 193–203.

Liu X (2008) Airborne LiDAR for DEM generation: Some critical issues. *Progress in Physical Geography* 32(1): 31–49.

McGranahan G, Balk D, and Anderson B (2007) The rising tide: Assessing the risks of climate change and human settlements in low elevation coastal zones. *Environment and Urbanization* 19(1): 17–37.

Marcy D, Brooks W, Draganov K, et al. (2011) New mapping tool and techniques for visualizing sea level rise and coastal flooding impacts. In: Wallendorf L, Jones C, and Ewing L, et al. (eds) *Proceedings of the 2011 Solutions to Coastal Disasters Conference, Anchorage, Alaska, 26–29 June*. Reston, VA: American Society of Civil Engineers, 474–490.

Marfai M and King L (2008) Potential vulnerability implications of coastal inundation due to sea level rise for the coastal zone of Semarang city, Indonesia. *Environmental Geology* 54(6): 1235–1245.

Meehl G, Stocker T, Collins W, et al. (2007) Global climate projections. In: Solomon S, Qin D and Manning M (eds) *Climate Change 2007: The Physical Science Basis. Contribution of Working Group I to the Fourth Assessment Report of the Intergovernmental Panel on Climate Change*. Cambridge: Cambridge University Press, Chapter 10.

Merwade V, Olivera F, Arabi M, et al. (2008) Uncertainty in flood inundation mapping: Current issues and future directions. *Journal of Hydrologic Engineering* 13(7): 608–620.

Mitsova D, Esnard A, and Li Y (2012) Using dasymteric mapping techniques to improve the spatial accuracy of

sea level rise vulnerability assessments. *Journal of Coastal Conservation* 16(3): 355–372.

Myers E, Wong A, Hess K, et al. (2005) Development of a National VDatum, and its application to sea level rise in North Carolina. In: *Proceedings of the 2005 US Hydrographic Conference, San Diego, CA, 28–31 March*.

National Digital Elevation Program (NDEP) (2004) Guidelines for digital elevation data, Version 1.0. Available at: www.ndep.gov/NDEP_Elevation_Guidelines_Ver1_10May2004.pdf.

National Oceanic and Atmospheric Administration (NOAA) (2001) Tidal datums and their applications. NOAA special publication NOS CO-OPS 1. Available at: http://tidesandcurrents.noaa.gov/publications/tidal_datums_and_their_applications.pdf.

National Oceanic and Atmospheric Administration (NOAA) (2003) Computational techniques for tidal datums handbook. NOAA special publication NOS CO-OPS 2. Available at: http://tidesandcurrents.noaa.gov/publications/Computational_Techniques_for_Tidal_Datums_handbook.pdf.

National Oceanic and Atmospheric Administration (NOAA) (2008) Topographic and bathymetric data considerations: Datums, datum conversion techniques, and data integration; Part II of a roadmap to a seamless topobathy surface. Report no. NOAA/CSC/20718-PUB, October. Available at: www.csc.noaa.gov/digitalcoast/_/pdf/considerations.pdf.

National Oceanic and Atmospheric Administration (NOAA) (2010a) *Adapting to Climate Change: A Planning Guide for State Coastal Managers*. NOAA Office of Ocean and Coastal Resource Management. Available at: http://coastalmanagement.noaa.gov/climate/adaptation.html.

National Oceanic and Atmospheric Administration (NOAA) (2010b) *Mapping Inundation Uncertainty*. NOAA Coastal Services Center. Available at http://www.csc.noaa.gov/beta/slr/assets/pdfs/Elevation_Mapping_Confidence_Methods.pdf.

National Oceanic and Atmospheric Administration (NOAA) (2010c) Technical considerations for use of geospatial data in sea level change mapping and assessment. NOAA NOS Technical Report, September. Available at: www.csc.noaa.gov/publications/slc_tech.pdf.

National Oceanic and Atmospheric Administration (NOAA) (2011) LiDAR quality assurance (QA) report. San Francisco Bay LiDAR project. NOAA Coastal Services Center. Available at: ftp://ftp.csc.noaa.gov/pub/crs/beachmap/qa_docs/ca/san_francisco_bay/SF_QA_Report_3rdDelivery_110420_Final.pdf.

National Oceanic and Atmospheric Administration (NOAA) (2012) Estimation of vertical uncertainties in VDatum. Available at: http://vdatum.noaa.gov/docs/est_uncertainties.html#toppage.

National Research Council (NRC) (2007) *Elevation Data for Floodplain Mapping*. Washington, DC: The National Academies Press.

National Research Council (NRC) (2012) *Sea-Level Rise for the Coasts of California, Oregon, and Washington: Past, Present, and Future*. Washington, DC: The National Academies Press.

Nicholls RJ (2011) Planning for the impacts of sea level rise. *Oceanography* 24(2): 144–157.

Parker B (2002) The integration of bathymetry, topography and shoreline and vertical datum transformations behind it. *International Hydrographic Review* 3: 14–26.

Parker B, Hess K, Milbert D, et al. (2003) A national vertical datum transformation tool. *Sea Technology* 44(9): 10–15.

Pfeffer W, Harper J, and O'Neel S (2008) Kinematic constraints on glacier contributions to 21st century sea level rise. *Science* 321(5894): 1340–1343.

Poulter B and Halpin P (2008) Raster modeling of coastal flooding from sea-level rise. *International Journal of Geographic Information Science* 22(2): 168–182.

Purvis M, Bates P, and Hayes C (2008) A probabilistic methodology to estimate future coastal flood risk due to sea level rise. *Coastal Engineering* 55(12): 1062–1073.

Raber G, Jensen J, Hodgson M, et al. (2007) Impact of lidar nominal post-spacing on DEM accuracy and flood zone delineation. *Photogrammetric Engineering and Remote Sensing* 73(7): 793–804.

Rahmstorf S (2007) A semi-empirical approach to projecting future sea-level rise. *Science* 315(5810): 368–370.

Rahmstorf S (2010) A new view on sea level rise. *Nature Reports Climate Change* 4: 44–45.

Rahmstorf S (2012) Sea-level rise: Towards understanding local vulnerability. *Environmental Research Letters* 7: 021001.

Rahmstorf S, Cazenave A, Church J, et al. (2007) Recent climate observations compared to projections. *Science* 316(5825): 709.

Rahmstorf S, Perrette M, and Vermeer M (2011) Testing the robustness of semi-empirical sea level projections. *Climate Dynamics* 34(3–4): 861–875.

Reynolds M, Berkowitz P, Courtot KN, et al. (eds) (2012) Predicting sea-level rise vulnerability of terrestrial habitat and wildlife of the Northwestern Hawaiian Islands. US Geological Survey Report no. 2012–1182.

Rignot E, Velicogna I, van den Broeke M, et al. (2011) Acceleration of the contribution of the Greenland and Antarctic ice sheets to sea level rise. *Geophysical Research Letters* 38: L05503.

Rosso P, Ustin S, and Hastings A (2006) Use of lidar to study changes associated with spatina invasion in San Francisco Bay marshes. *Remote Sensing of Environment* 100: 295–306.

Rotzoll K and Fletcher C (2013) Assessment of groundwater inundation as consequence of sea-level rise. *Nature Climate Change* 3: 477–481.

Schmid K, Hadley B, and Wijekoon N (2011) Vertical accuracy and use of topographic lidar data in coastal marshes. *Journal of Coastal Research* 27(6A): 116–132.

Shen J and Toth CK (eds) (2009) *Topographic Laser Ranging and Scanning: Principles and Processing*. Boca Raton, FL: CRC Press.

Sithole G and Vosselman G (2004) Experimental comparison of filter algorithms for bare-Earth extraction from airborne laser scanning point clouds. *ISPRS Journal of Photogrammetry and Remote Sensing* 59: 85–101.

Slangen A, Katsman C, van de Wal R, et al. (2012) Towards regional projections of twenty-first century sea-level change based on IPCC SRES scenarios. *Climate Dynamics* 38(5–6): 1191–1209.

Strauss B, Ziemlinski R, Weiss J, et al. (2012) Tidally adjusted estimates of topographic vulnerability to sea level rise and flooding for the contiguous United States. *Environmental Research Letters* 7: 014033.

Titus J and Richman C (2001) Maps of lands vulnerable to sea level rise: Modeled elevations along the US Atlantic and Gulf coasts. *Climate Research* 18: 205–228.

Vermeer M and Rahmstorf S (2009) Global sea level linked to global temperature. *Proceedings of the National Academy of Sciences of the United States of America* 106: 21527–21532.

Webster T, Forbes D, Dickie S, et al. (2004) Using topographic lidar to map flood risk from storm-surge events for Charlottetown, Prince Edward Island, Canada. *Canadian Journal of Remote Sensing* 30(1): 64–76.

Webster T, Forbes D, Mackinnon E, et al. (2006) Flood-risk mapping for storm-surge events and sea-level rise using lidar for southeast New Brunswick. *Canadian Journal of Remote Sensing* 32(2): 194–211.

Zhang K (2011) Analysis of non-linear inundation from sea-level rise using lidar data: A case study for South Florida. *Climatic Change* 106(4): 537–565.

Zhang K and Whitman D (2005) Comparison of three algorithms for filtering airborne lidar data. *Photogrammetric Engineering and Remote Sensing* 71: 313–324.

Zhang K, Dittmar J, Ross M, et al. (2011) Assessment of sea-level rise impacts on human population and real property in the Florida Keys. *Climatic Change* 107(1–2): 129–146.

Zhang K, Li Y, Liu H, et al. (2013) Comparison of three methods to estimate the sea level rise effect on storm surge flooding. *Climatic Change* 118(2): 487–500.

Zilkoski D, Richards J, and Young G (1992) Results of the general adjustment of the North American Vertical Datum of 1988. *Surveying and Land Information Systems* 52(3): 133–149.